International Journal of Nanomedicine

Dovepress
open access to scientific and medical research

Open Access Full Text Article

ORIGINAL RESEARCH

Antimicrobial potential of green synthesized CeO_2 nanoparticles from *Olea europaea* leaf extract

This article was published in the following Dove Press journal:
International Journal of Nanomedicine
4 October 2016
Number of times this article has been viewed

Qaisar Maqbool[1]
Mudassar Nazar[1]
Sania Naz[2]
Talib Hussain[3]
Nyla Jabeen[4]
Rizwan Kausar[5]
Sadaf Anwaar[4]
Fazal Abbas[6,7]
Tariq Jan[6]

[1]Department of Biotechnology, Virtual University of Pakistan, Lahore, Pakistan; [2]Department of Biotechnology, Quaid-i-Azam University, Islamabad, Pakistan; [3]National Institute of Vacuum Science and Technology (NINVAST), Islamabad, Pakistan; [4]Department of Biotechnology and Bioinformatics Lab., International Islamic University, Islamabad, Pakistan; [5]Department of Chemistry, University of Sargodha, Sargodha, Pakistan; [6]Department of Physics, International Islamic University, Islamabad, Pakistan; [7]Interdisciplinary Research Organization, University of Chakwal (UOC), Chakwal, Pakistan

Correspondence: Qaisar Maqbool
Department of Biotechnology, Virtual University of Pakistan, Off Raiwind Road, Lahore 54000, Pakistan
Tel +92 42 332 593 7838
Fax +92 42 543 540838
Email qaisar.vu@gmail.com

Talib Hussain
National Institute of Vacuum Science and Technology (NINVAST), NCP Complex Shah Dara Road, Islamabad 44000, Pakistan
Tel +92 51 903 8204
Fax +92 51 903 8204
Email thminhas7@yahoo.com

Abstract: This article reports the green fabrication of cerium oxide nanoparticles (CeO_2 NPs) using *Olea europaea* leaf extract and their applications as effective antimicrobial agents. *O. europaea* leaf extract functions as a chelating agent for reduction of cerium nitrate. The resulting CeO_2 NPs exhibit pure single-face cubic structure, which is examined by X-ray diffraction, with a uniform spherical shape and a mean size 24 nm observed through scanning electron microscopy and transmission electron microscopy. Ultraviolet-visible spectroscopy confirms the characteristic absorption peak of CeO_2 NPs at 315 nm. Fourier transform infrared spectroscopy reflects stretching frequencies at 459 cm^{-1}, showing utilization of natural components for the production of NPs. Thermal gravimetric analysis predicts the successful capping of CeO_2 NPs by bioactive molecules present in the plant extract. The antimicrobial studies show significant zone of inhibition against bacterial and fungal strains. The higher activities shown by the green synthesized NPs than the plant extract lead to the conclusion that they can be effectively used in biomedical application. Furthermore, reduction of cerium salt by plant extract will reduce environmental impact over chemical synthesis.

Keywords: XRD, SEM, TEM, FTIR, antibacterial, antifungal, nanomedicine, green fabrication

Introduction

Green synthesis of metallic oxide nanoparticles (NPs) is an emerging field of nanoscience and technology. Synthesis methodology and surface modification play a critical role in the physical, chemical, electrical, and optical properties of nanomaterials. Cerium oxide (CeO_2) is a semiconductor with a band gap energy of 3.0–3.9 eV and large excitation energy. In bulk form, CeO_2 is a singular rare earth oxide and does not show any crystallographic modifications by temperature increase up to its melting point.[1–5] Its various applications such as acting as a catalyst; use in sensor, solid oxide fuel cells, and sunscreen cosmetics; and its O_2 storage capacity, role in CO_2 solar conversion, and antibacterial applications are due to its idiosyncratic ability to alter the oxidation states.[6–10]

Ordinarily, CeO_2 NPs are fabricated by physical and chemical methods including hydrothermal,[11] flame spray pyrolysis,[12] thermal decomposition,[13] aqueous precipitation,[14] and coprecipitation technique.[15] In contrast, green synthesis of metallic oxide NPs offers several advantages such as cost-effectiveness, large-scale commercial production, and pharmaceutical applications. The CeO_2 NPs are considered less toxic toward cell lines, when compared to TiO_2 and ZnO.[16] Biosynthesis of CeO_2 NPs using plant extracts such as *Gloriosa superba* L. and *Hibiscus sabdariffa* has been reported[1] with promising results.

Olea europaea belongs to the family *Oleaceae* and is native to tropical and warm temperate regions of the world.[17] Mediterranean region serves as the major cultivation area,

accounting for about 98% of the world's olive production.[18] *O. europaea* exhibits antioxidant, anti-inflammatory, antiatherogenic, anticancer, antimicrobial, and antiviral activities, along with hypolipidemic and hypoglycemic potential.[19] Bioactive compounds principally present in olive leaves are oleuropein, followed by hydroxytyrosol, the flavone-7-glucosides of luteolin and apigenin, and verbascoside.[20,21]

This study reports green synthesis of CeO_2 NPs utilizing *O. europaea* leaf extract as an effective chelating agent without any acid or base treatment. The synthesized CeO_2 NPs are further characterized for their antibacterial and antifungal potential.

Experimental procedures

Collection and processing of plant material

The authenticated *O. europaea* leaves were procured from Barani Agricultural Research Institute, Chakwal, Pakistan. Fresh leaves were washed with distilled water and air-dried under shade at room temperature to avoid photodissociation of bioactive compounds. For extract preparation, 20 g of dried leaves was ground and suspended in 200 mL of distilled water. The mixture was placed in a shaking incubator at 50°C for 2 hours at 50 rpm. Thereafter, it was filtered using Whatman No 1 filter paper and the filtrate was stored at room temperature for further usage.

Fabrication of CeO_2 NPs by *O. europaea* leaf extract

For green synthesis of CeO_2 NPs, 8.68 g of $Ce(NO_3)_3 \cdot 6H_2O$ was added to 200 mL of *O. europaea* leaf extract and stirred on a magnetic hotplate at 50°C, 1,500 rpm for 2 hours. The blackish brown CeO_2 NPs were collected by centrifugation at 10,000 rpm (GR BioTek, Orpington, England) for 10 minutes. The NPs were washed repeatedly with deionized water and finally dried in hot air oven at 60°C for ~6 hours and further annealed in Gallenkamp furnace (Apeldoorn, the Netherlands) at 500°C for 2 hours. The yellow-colored NPs obtained were stored in an air-tight jar at room temperature. A schematic diagram for the fabrication of CeO_2 NPs using *O. europaea* leaf extract is shown in Figure 1.

Characterization of CeO_2 NPs

Scanning electron microscopy (SEM)

The size and shape of synthesized CeO_2 NPs were studied using JEOL-JSM-6490LA SEM (JEOL, Tokyo, Japan) operating at 20 kV with a counting rate of 2,838 cps.

Transmission electron microscopy (TEM)

To further investigate the internal morphology, TEM analysis of green fabricated CeO_2 NPs was performed by TEM (model no JEOL-1010) operating at 80 kV.

X-ray diffraction (XRD; crystallographic structure)

To examine the crystallographic structure of green synthesized CeO_2 NPs, XRD analysis was carried out using X'Pert³ Powder (PANalytical) with nickel monochromator in the range of 2θ from 20° to 80° using Cu Kα radiation of wavelength 1.5406 Å. Operating voltage of 40 kV with 30 mA current was provided at room temperature. To calculate the theoretical size of CeO_2 NPs, Scherrer's equation ($D=0.9\lambda/\beta \cos\theta$) was employed, where D is the average crystalline domain size perpendicular to the reflecting planes, λ the X-ray wavelength (1.5406 Å), β the angular full width at half maximum in radians, and θ is the diffraction angle (2θ is the measured angle of diffraction in degrees) or Bragg's angle.

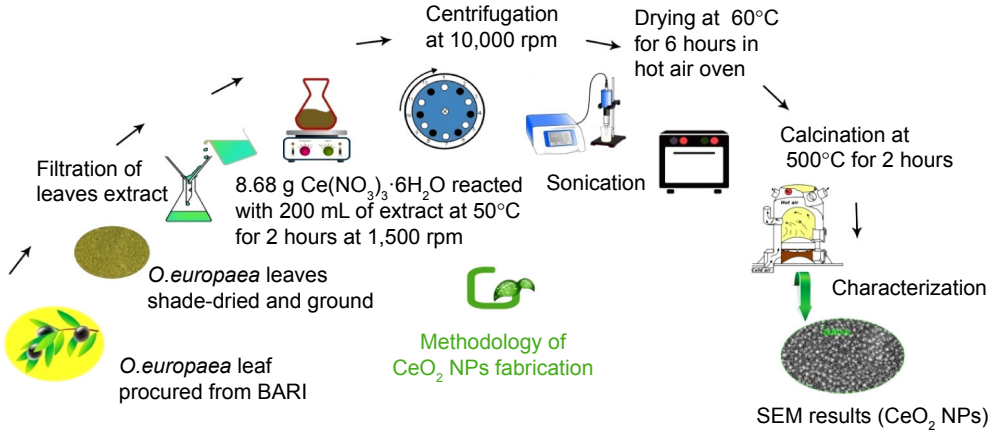

Figure 1 Schematic diagram of fabrication of CeO_2 NPs using *Olea europaea* leaf extract.
Abbreviations: BARI, Barani Agricultural Research Institute; NPs, nanoparticles; SEM, scanning electron microscopy; *O. europaea, Olea europaea*.

Furthermore, the lattice constant was measured using the following equation:

$$d = \frac{a}{\sqrt{h^2 + k^2 + I^2}}$$

where $a=b=c$ are lattice constants, d represents the interplanner spacing which was calculated by using $2d \sin\theta = n\lambda$, and h, k, and I are Miller indices. The unit cell volume was calculated using $V=a^3$ formula unit.

Fourier transform infrared (FTIR) spectroscopy

For the identification of unknown bio-active compounds in plant extract, utilization of capping agents from plant extract and confirmation of production materials (CeO_2 NPs), FTIR spectroscopic analysis was performed using KBr pellet methodology (model SHIMADZU FTIR, Kyoto, Japan) in the wavenumber ranges 400–4,000 cm^{-1}. FTIR spectra for CeO_2 NPs, residue (as synthesized), and *O. europaea* leaf extract were recorded separately and explained comparatively.

Ultraviolet (UV)-visible spectroscopy

The optical characterization of green fabricated CeO_2 NPs was made through UV-visible spectroscopy in the range of 290–400 nm with a Shimadzu spectrophotometer (model UV-1800, Kyoto, Japan) operating at a resolution of 1 nm. Three milligrams of synthesized CeO_2 NPs was dissolved in 10 mL of deionized H_2O and this solution was sonicated for 20 minutes. Subsequently, the liquid sample was subjected to UV-visible spectrophotometry.

Thermal gravimetric analysis (TGA)

To examine the thermal properties and capping action of bioactive compounds for tailoring CeO_2 NPs, we performed TGA (model Diamond TGA; PerkinElmer, Waltham, USA) under nitrogen environment from 25°C to 800°C at 10°C/minute.

Antibacterial activity of CeO_2 NPs

The antibacterial activities of green synthesized CeO_2 NPs were studied against Gram-positive (G+ve) (*Staphylococcus aureus* ATCC 6538) and Gram-negative (G–ve) (*Escherichia coli* ATCC 15224, *Pseudomonas aeruginosa* ATCC 15442, *Klebsiella pneumoniae* ATCC-BAA 1706) strains by disk diffusion method with slight modification.[1] In brief, the bacterial strains were cultured in nutrient broth (Sigma-Aldrich Co., St Louis, MO, USA) at 37°C until the culture reached 1.5×10^8 colony forming units (CFU) per milliliter. About 20 mL of autoclaved molten nutrient agar was poured into the Petri dishes and allowed to cool. All of the four bacterial cultures were swapped over solidified agar medium. Disks were loaded with 20 µg/5 µL CeO_2 NPs solution. A solution of cefixime or roxithromycin (4 mg/mL each) was used as positive control and deionized H_2O as negative control. The plates were incubated at 37°C for 24 hours and the zones of inhibition (ZOIs) around the disks were measured thereafter.

Antifungal assay

Antifungal activity was determined against *Mucor* species (FCBP-0300), *Aspergillus flavus* (FCBP-0064), *Fusarium solani* (FCBP-434), and *Aspergillus niger* (FCBP-0198) by disk diffusion method. Sabouraud dextrose agar (pH 5.7) (Sigma-Aldrich Co.) was autoclaved and poured in Petri plates ensuring sterile conditions. Fungal lawns were prepared by inoculating spores on the surface of the growth media. Thereafter, disks were loaded with CeO_2 NPs solution 20 µg/5 µL through micropipette. Clotrimazole 10 µg/disk was used as positive control, while deionized water served as negative control. The plates were incubated at 25°C for 24–48 hours and ZOI was measured.

CFU counting assay

To examine the percentage reduction in bacterial count with time, we carried out CFU counting assay. The experimentation was performed in sample tubes, each having 2 mL of sterilized (autoclaved) nutrient broth. The first sample tube containing 2 mL of nutrient broth acted as sterile negative control and the second tube was impregnated with cefixime (as positive control), while the remaining four samples were inoculated with *S. aureus* (G+ve), and *E. coli*, *P. aeruginosa*, and *K. pneumoniae* (G–ve), respectively, having a concentration of 10^7 and 10^9 CFU/mL each, and then placed in a shaking incubator at 37°C. Thereafter, the bacterial culture tubes were loaded with CeO_2 NPs solution (20 µg/5 µL). After an interval of 30 minutes, 10 µL from each sample was collected and spread over the already prepared agar plate surface. To estimate the bacterial colony in liquid, McFarland turbidity standards were applied, and their values were calibrated before and after incubation. Positive and negative control tests were performed on *E. coli* only. Later on, the plates were incubated at 37°C and the percentage reduction with time in bacterial count was calculated by the following approximation:[22]

$$\%\ \text{reduction} = \frac{\text{Viable count at 0 minutes} - \text{Viable count at 150 minutes}}{\text{Viable count at 0 minutes}} \times 100$$

Statistical analysis

Results are calculated as the mean of at least three individual experiments presented with standard deviation (SD). The statistical analysis of the results was carried out with Student's *t*-tests by using Statistical Package for the Social Sciences software package version 19.0 (IBM Corporation, Armonk, NY, USA) and considered significant at *P*-values <0.05.

Results and discussion

Biosynthesis process using *O. europaea* leaf extract (visual observations)

Synthesis of NPs using plant extracts has several advantages over other conventional biosynthesized routes (based on fungi, bacteria, etc). It is because the green extract is more ecofriendly and environment friendly, and fewer cytotoxic reducing agents are required for tailoring NPs. It is also commonly observed that maintaining microbial cultures under optimum conditions is time consuming and costly. In bulk (at an industrial level), safe mode synthesis of NPs, microbial-based NPs production has its own limitations.[23,24]

O. europaea aqueous extract contains a variety of molecules that might be effectively utilized as chelating agents in the green synthesis of CeO_2 NPs. Upon addition of $(CeNO_3)_3$ $6H_2O$, the biologically active compounds of the plant extract[21] act as reducing agents for the nanofabrication process. Oleuropein is the most abundant bioactive compound in *O. europaea* aqueous extract, which breaks down into highly polarizable and reactive hydroxytyrosol.[21] It may take part in the redox mechanism in tuning CeO_2 NPs, as shown in Figure 2. Figure 3 shows the change in color from dark blackish green to dirty green, indicating the formation of CeO_2 NPs. The blackish brown CeO_2 NPs were collected by centrifugation at 10,000 rpm for about 10 minutes. Thereafter, the NPs were washed repeatedly with deionized water to eliminate the uncoordinated biomolecules from the extract, and finally dried in hot air oven at 60°C for ~6 hours and further annealed at 500°C for 2 hours. The yellow-colored NPs obtained were stored at room temperature. The entire recovery process is presented in Figures 1 and 2.

SEM analysis

Figure 4 depicts the SEM images of green synthesized CeO_2 NPs. It is obvious from the SEM micrograph that the CeO_2 NPs are highly homogeneous and symmetrical in morphology with spherical shape, and the findings clearly represent

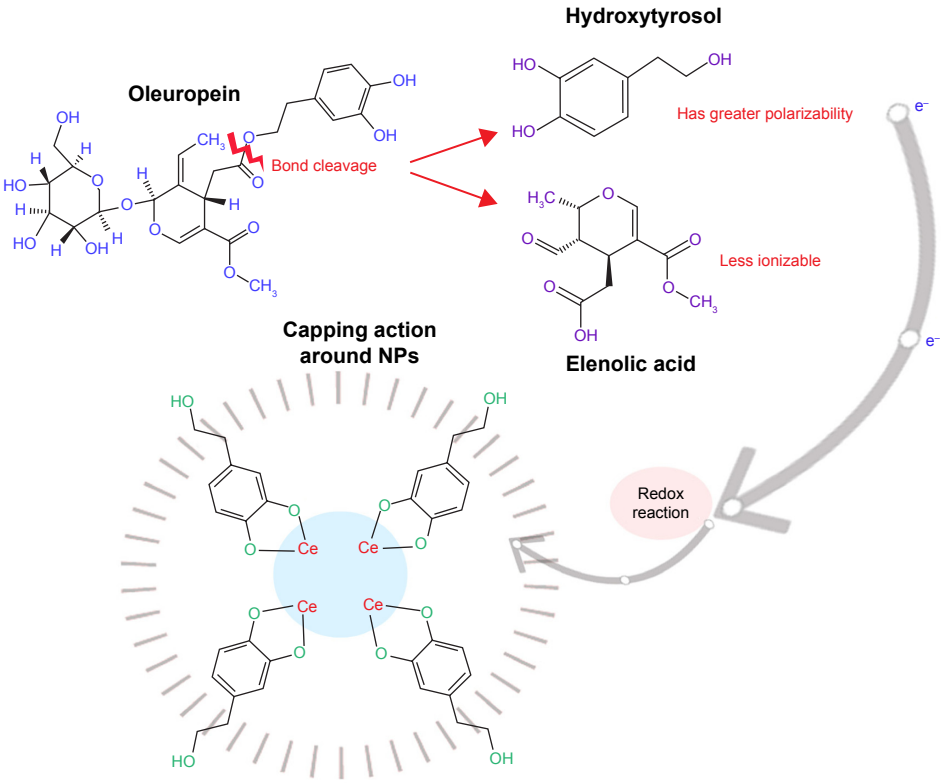

Figure 2 Hypothesized redox process of CeO_2 NPs synthesis.
Abbreviation: NPs, nanoparticles.

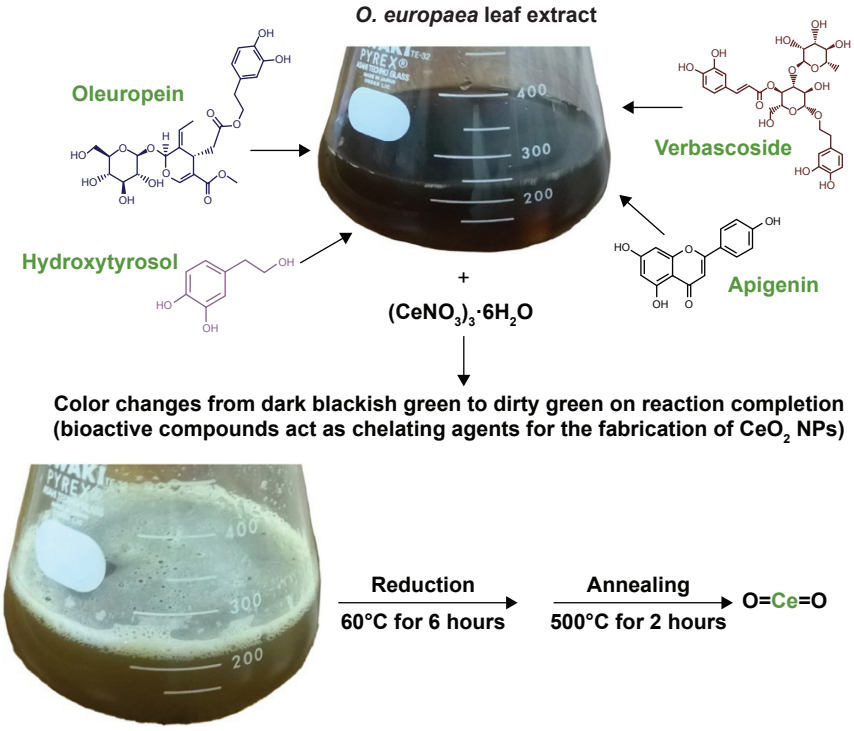

Figure 3 Biosynthesis of CeO_2 NPs.
Abbreviations: NPs, nanoparticles; *O. europaea, Olea europaea*.

a mean size of 24 nm. Similar morphological shape with uniform average grain size of less than 30 nm was also reported previously.[10,25,26]

TEM analysis

It is clear from the TEM micrograph that the green synthesized CeO_2 NPs exhibit spherical morphology with highly homogeneous symmetry and an average particle size of 24 nm (Figure 5).

XRD (crystallographic structure) analysis

Figure 6 shows the XRD profile of green fabricated CeO_2 NPs. It shows that the CeO_2 NPs possess single-phase cubic fluorite structure without any additional peaks. Presence of several broad Bragg peaks corresponds to (111), (200), (220), (311), (222), (400), (331), and (420) orientations and they are precisely well indexed to Joint Committee on Powder Diffraction Standards (JCPDS) (card no 34-0394). This later crystallographic phase reflects that each cerium site

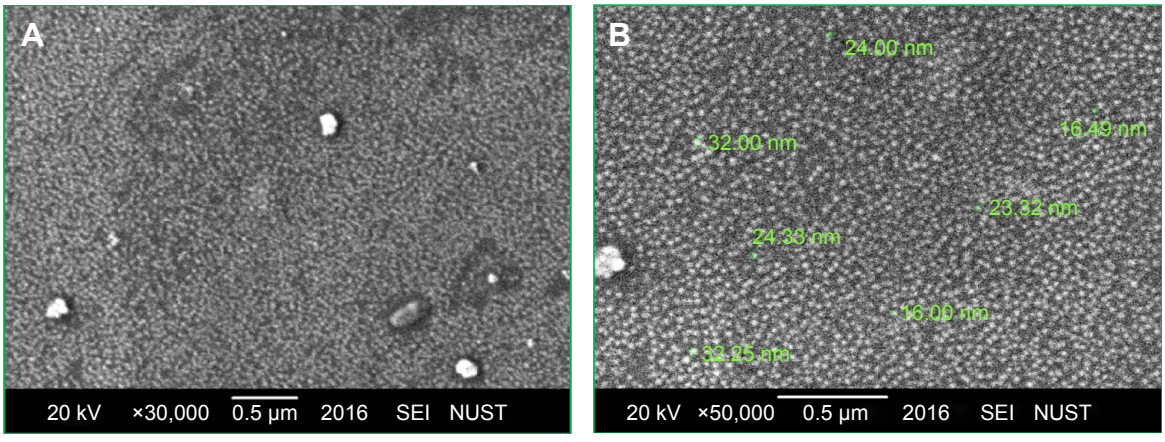

Figure 4 SEM images of green synthesized CeO_2 NPs. (**A**) Magnification ×30,000; (**B**) Magnification ×50,000.
Abbreviations: NPs, nanoparticles; SEM, scanning electron microscopy; SEI, scanning electron-microscopy instrument; NUST, National University of Sciences and Technology.

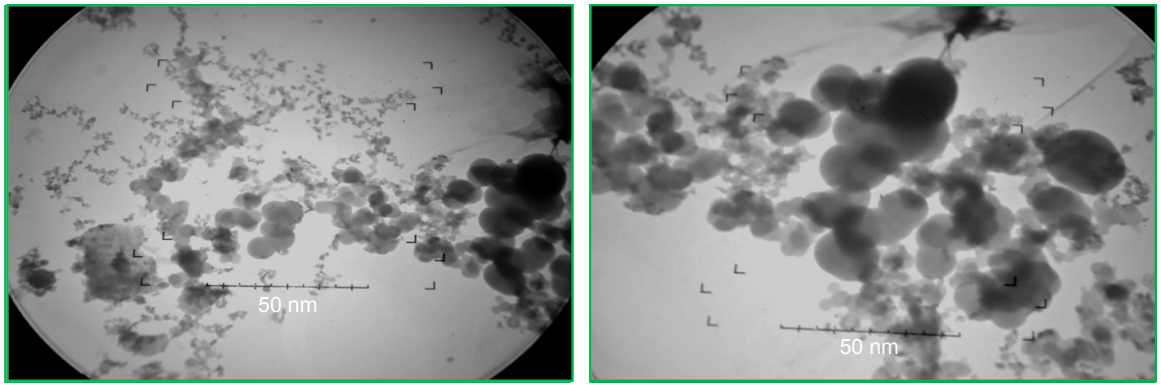

Figure 5 TEM micrographs of green synthesized CeO_2 NPs.
Abbreviations: NPs, nanoparticles; TEM, transmission electron microscopy.

is encountered by eight oxygen sites in face-centered cubic arrangement, while each oxygen has the geometry of tetrahedron cerium site. Using Debye–Scherrer approximation and from the broadening of peaks, the approximate crystallite size of CeO_2 NPs was found to be 6 nm, which shows that each grain of size 24 nm was composed of a cluster of 6 nm crystallites. The observed value was found to be close to that reported previously.[25] The calculated value of lattice constant "a" is 0.585 nm, while the unit cell volume "V" is measured to be 0.20 nm.

FTIR spectroscopy analysis

Comparative FTIR results illustrate significant absorption peaks in the wave number range 400–4,000 cm^{-1} (Figure 7). The range between 2,500 and near 4,000 cm^{-1} is assigned to O–H and C–H stretch. The plant extract exhibiting N–O symmetric stretch at 1,355 cm^{-1} was found to be less in the residue after CeO_2 NPs were isolated, reflecting that Ce is actively oxidized to CeO_2 by the nitro compounds in extract chemistry. The onset of a broad intense band that can be viewed as one tends toward higher vibrations (2,800 cm^{-1}) can be ascribed to O–H stretching range due to the presence

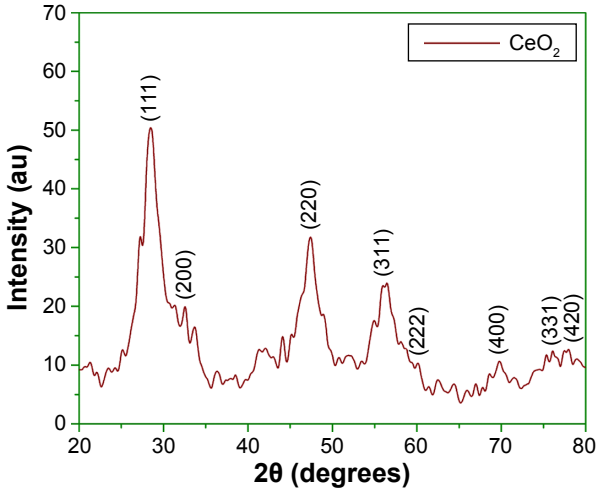

Figure 6 Typical XRD analysis of CeO_2 NPs at room temperature.
Abbreviations: NPs, nanoparticles; XRD, X-ray diffraction.

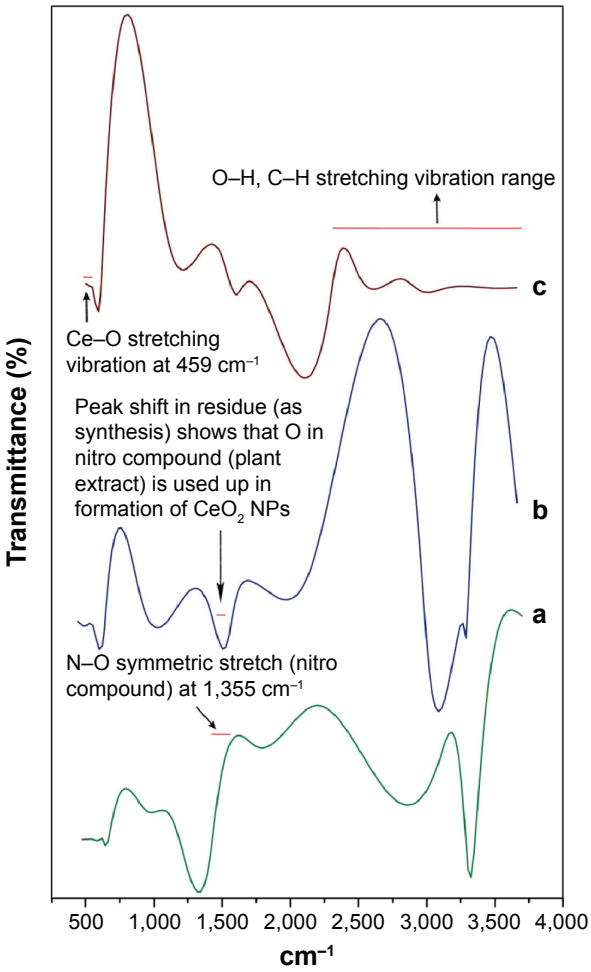

Figure 7 FTIR spectra of biosynthesized CeO_2 NPs from *Olea europaea* leaf extract.
Notes: (**a**) Plant extract; (**b**) residue (as synthesized); (**c**) CeO_2 NPs.
Abbreviations: FTIR, Fourier transform infrared; NPs, nanoparticles.

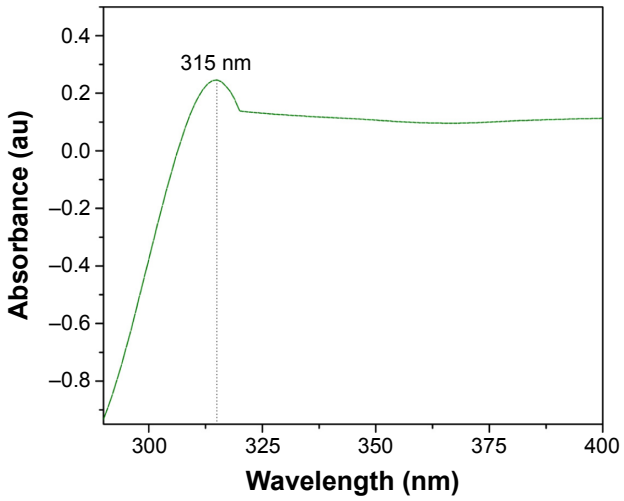

Figure 8 UV-Vis spectra of CeO_2 NPs.
Abbreviations: NPs, nanoparticles; UV-Vis, ultraviolet-visible spectroscopy.

of surface-adsorbed water molecules from the surroundings.[27] The spectra due to stretching frequency of Ce–O can be seen at 459 cm^{-1}, which indicates the fabrication of CeO_2 NPs. Similarly, Ce–O stretching band at 451 cm^{-1} and at 450 cm^{-1} was reported by Arumugam et al[10] and Goharshadi et al,[28] respectively.

UV-visible spectroscopy studies

Figure 8 illustrates the UV-visible absorption spectra of CeO_2 NPs, which demonstrates the presence of a single intensified peak at 315 nm that was also closely observed in previous studies.[25] The position of the absorption peak confirms that green synthesized CeO_2 NPs possess fluorite cubic morphology,[26] as justified in Figures 4 and 5.

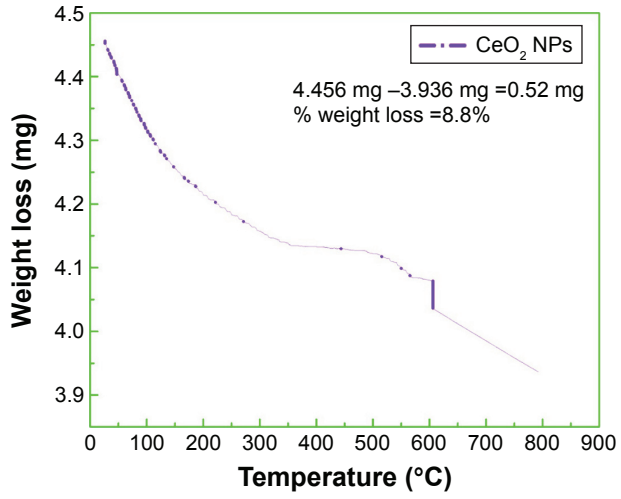

Figure 9 TGA curve of green synthesized CeO_2 NPs.
Abbreviations: NPs, nanoparticles; TGA, thermal gravimetric analysis.

TGA studies

TGA of biosynthesized CeO_2 NPs was performed to study the capping action of biomolecules and the thermal behavior of the synthesized CeO_2 NPs, which is shown in Figure 9. TGA represents different stages of decomposition. Weight loss occurring in the first step at temperatures from 25°C to 115°C was ascribed to the loss of surface water molecules.[29] The minor weight loss that occurred in the second step at temperatures from 50°C to 200°C was due to the combustion of bioactive surface organic components acting as capping agents. The slight weight loss occurring at around 600°C was because of oxygen loss at high temperature.[30] Our experimental observations show total weight loss of 0.52 mg (8.8%) of the sample.

Antibacterial analysis of CeO_2 NPs

The antibacterial assay was performed against G+ve and G–ve bacterial entities using CeO_2 NPs sample loaded at a concentration of 20 µg/05 µL on disks. Figure 10 reflects the measurements in size of ZOI around CeO_2 NPs poured disks. In the case of *K. pneumoniae, S. aureus*, and *P. aeruginosa*, a ZOI of 9, 10, and 8 mm was observed, respectively, which shows mild to moderate antibacterial behavior. Promising ZOI of 19 mm was recorded against *E. coli*; the prominent difference in ZOI might be due to the unique cell membrane structure that helps the bacterium to resist antimicrobial agents. Besides all these, other features such as the rate at which the NPs diffuse also play an important role against various bacterial strains.[31] Figure 10 shows that G+ve bacteria are more susceptible to CeO_2 NPs than G–ve bacteria;

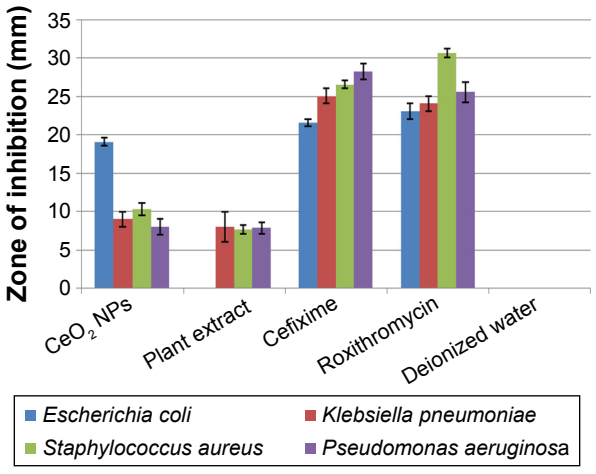

Figure 10 Antibacterial analysis of CeO_2 NPs, plant extract, cefixime/roxithromycin (positive control), and deionized water (negative control), taking their mean values with ±SD.
Abbreviations: NPs, nanoparticles; SD, standard deviation.

similar trends were reported before.[10] Green synthesized NPs have proven efficiency and comparatively low genotoxic and cytotoxic behavior toward healthy cells, when compared to NPs synthesized by various chemical methods.[32] CeO_2 NPs fabricated by way of chemical methods were also found to be cytotoxic to somatic cells.[25] *O. europaea* leaf extract also takes part in inhibiting *K. pneumoniae, S. aureus*, and *P. aeruginosa*, with ZOI of 8, 7.6, and 7.8 mm, respectively; its potential activity has also been reported in previous studies.[33,34] Bioactive compounds from the leaf extract, such as oleuropein, are also found to be magically active in inhibiting several bacterial pathogens.[34]

From the results of XRD, SEM, and TEM, the average CeO_2 NP size was found to be 24 nm, with the smaller crystallite size being 6 nm. Higher surface area due to smaller crystal size results in greater antibacterial activity.[35] The antibacterial activity of CeO_2 NPs primarily depends upon the electrostatic attraction between positively charged NPs and negatively charged bacterial cell surface and is crucial for the activity of NPs as a bactericidal agent. The interaction is also responsible for reactive oxygen species (ROS) generation, which ultimately leads to bactericidal effect.[36,37] ROS include the highly reactive hydroxyl radical (OH), singlet oxygen ($_1O^2$), and the least toxic superoxide anion radical ($^-{}^*O_2$), contributing to the major oxidative stress in biological systems.[38] ROS production is closely related to the efficiency of a photocatalyst, depending on the generation rate, rate of migration, and energy levels of the photoexcited electron–hole pairs. In the present study, such an increase in ROS levels is perhaps linked to the electronic and microstructure properties like grain size, specific surface area, pore size, and so on. The mechanism of photoexcited generation of ROS can be given as follows:[10]

$$CeO_2 + h\upsilon \rightarrow e^- + h^+h^+ + H_2O \rightarrow \cdot OH + H + e^- + O_2$$
$$\rightarrow O_2\ ^-O_2 + H^+ \rightarrow HO_2\ \cdot HO_2 + H^+ + e^- \rightarrow H_2O_2$$

Mostly, it is believed that NPs release ions which interact with the thiol (–SH) group of the protein residing at the bacterial cell surface,[39] resulting in denaturation of surface protein along with loss of cell membrane permeability, ultimately causing cell death. The rough surface for metallic NPs also intensifies their mechanical bactericidal capabilities of *E. coli*.[40] In our experimentation, UV analysis showed strong, intensified CeO_2 NPs absorption peaks at 315 nm. It is a well-known fact that Ce, as compared to its bulk, forms low band gap energy which results in its photoexcitation at room temperature.[25] This phenomenon will also assist in mass production of ROS inside bacterial cellular environment, and intoleration of ROS due to CeO_2 NPs results in malfunctioning of microbial biosynthetic machinery, causing lethality. In Figure 11 is presented a possible schematic diagram summarizing the above fact.

Antifungal assay analysis of CeO_2 NPs

The antifungal properties of green synthesized CeO_2 NPs have been shown in Figure 12. *A. flavus* and *A. niger* show greater CeO_2 NPs susceptibility with ZOI of 19 mm than *F. solani* for which the ZOI is 10 mm. The fungicidal activity of CeO_2 NPs was found to be maximum in the case of *Mucor* species with ZOI of 22 mm, showing great competency as an antifungal agent, like other antifungal candidates.[41] The

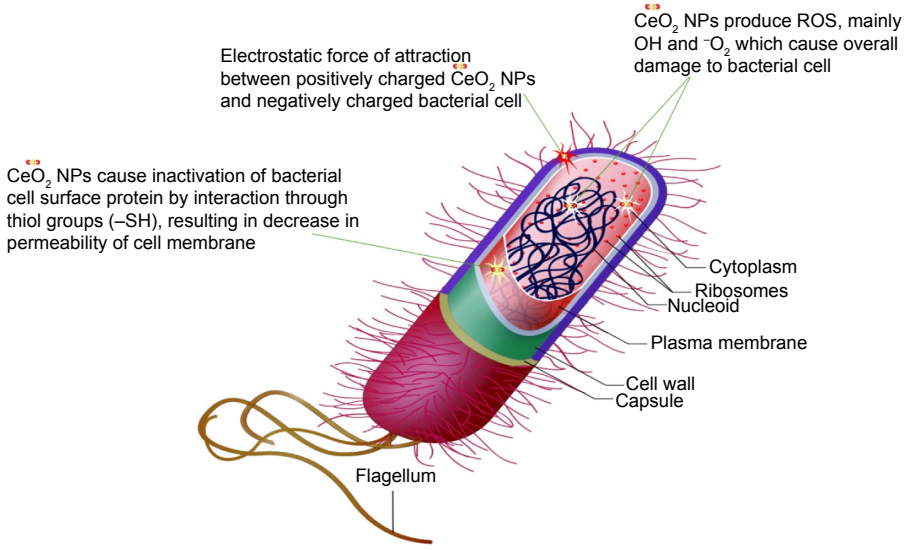

Figure 11 Schematic illustration of CeO_2 NPs antibacterial activity.
Abbreviations: NPs, nanoparticles; ROS, reactive oxygen species.

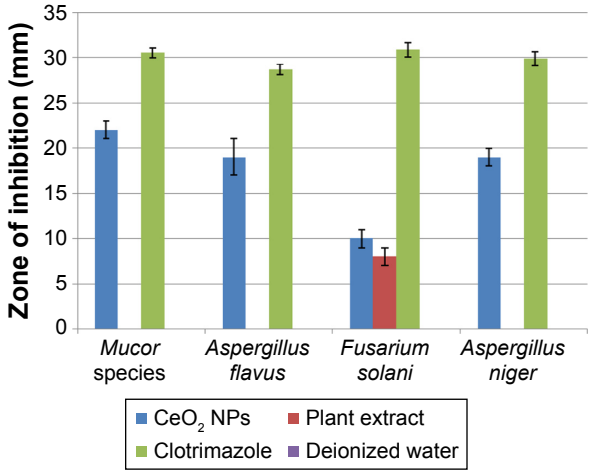

Figure 12 Antifungal analysis of CeO_2 NPs, plant extract, clotrimazole (positive control), and deionized water (negative control), taking their mean values with ±SD.
Abbreviations: NPs, nanoparticles; SD, standard deviation.

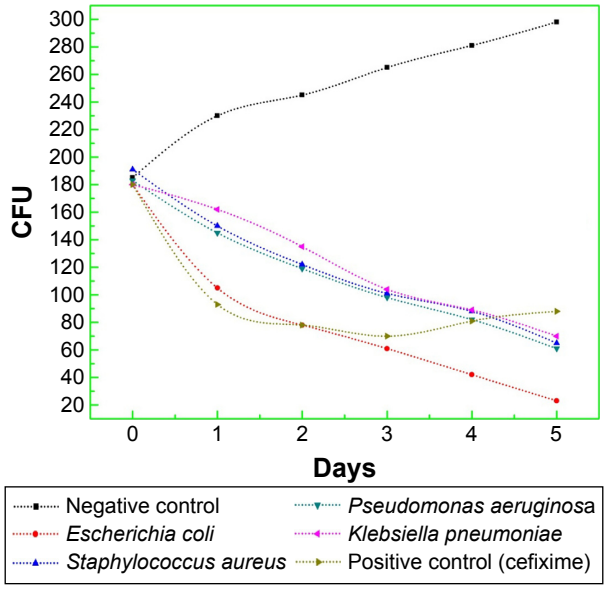

Figure 13 CFU counting assay of green synthesized CeO_2 NPs against G+ve and G–ve bacterial strains.
Abbreviations: CFU, colony forming units; G+ve, Gram positive; G–ve, Gram negative; NPs, nanoparticles.

exact mechanism of the antifungal activity of CeO_2 NPs is not understood, but the antimicrobial potential is probably due to the electromagnetic interaction and ROS generation,[36] like the production of lethal hydroxyl radical (OH) when present in the immediate vicinity of the lipid membrane. ROS cause oxidative deterioration of cell membrane lipids,[42] denaturing the cell membrane permeability with leakage of potassium ions, ultimately causing cell death.[39]

Analysis of CFU counting assay

The results of progression in bacterial growth with time are documented in Figure 13. It is obvious that for all samples, the bacterial population was in lag phase during the first 20 minutes of the experiment, but with the addition of CeO_2 NPs (20 µg/5 µL), persistent decline in growth was observed. Reduction in viability of *E. coli* was markedly maximum, while for all other bacterial strains, the growth inhibition rate with time was almost similar. So, it is very clear that due to extremely small particle size and pure phase crystallinity with high surface area (Figures 4 and 5), CeO_2 NPs exhibit prominent bacteriostatic and bactericidal activity. This might be due to intolerance of metallic CeO_2 NPs by bacterial metabolic machinery, lethal ROS generation, and greater cytotoxicity toward microbial pathogens.[36,37] Future work regarding the molecular level interaction of CeO_2 NPs in bacterial growth inhibition needs more exploration.

Conclusion

The leaf extract of *O. europaea* is proved to be an effective chelating agent for the green synthesis of highly homogeneous, ecofriendly, and extremely small sized CeO_2 NPs. Both XRD and SEM findings confirm the cubic fluorite structure of CeO_2 NPs without any impurities and with a mean crystallite size of 6 nm and an average grain size of 24 nm. FTIR results reveal discharge of bioactive compounds from the leaf extract and Ce–O stretching mode at 459 cm^{-1}. This study shows that CeO_2 NPs exhibit mild to moderate antibacterial activity against both G+ve and G–ve strains, especially high susceptibility was shown by *E. coli*. CeO_2 NPs exhibited promising inhibitory effect against *Mucor* species, ensuring their antifungal properties. It can be deduced from this study that CeO_2 NPs synthesized through green chemistry have great potential for future antimicrobial therapies. The follow-up study will focus on differential cytotoxic behavior of photosynthesized CeO_2 NPs to healthy and cancer cells; more specifically, the size-dependent anticancer and antimicrobial properties will be examined.

Acknowledgments

The authors acknowledge Sidra Iftikhar (Department of Mathematics, University of Wah, Pakistan) for providing technical assistance regarding SEM and XRD operations.

Disclosure

The authors report no conflicts of interest in this work.

References

1. Thovhogi N, Diallo A, Gurib-Fakim A, Maaza M. Nanoparticles green synthesis by Hibiscus Sabdariffa flower extract: main physical properties – university of South Africa. *J Alloys Compd*. 2015;647:392–396.

2. Chandrakala HN, Ramaraj B, Shivakumaraiah, Siddaramaiah. Optical properties and structural characteristics of zinc oxide cerium oxide doped polyvinyl alcohol films. *J Alloys Compd*. 2014;586:333–342.
3. Chen JC, Chen WC, Tien YC, Shih CJ. Effect of calcination temperature on the crystallite growth of cerium oxide nano-powders prepared by the co-precipitation process. *J Alloys Compd*. 2010;496(1–2): 364–369.
4. Lee B-H, Nakayama T, Tokoi Y, Suzuki T, Niihara K. Synthesis of CeO/TiO nanoparticles by laser ablation of Ti target in cerium (III) nitrate hexahydrate (Ce(NO)·6HO) aqueous solution. *J Alloys Compd*. 2010;509(4):1231–1235.
5. Gangopadhyay S, Frolov DD, Masunov AE, Seal S. Structure and properties of cerium oxides in bulk and nanoparticulate forms. *J Alloys Compd*. 2014;584:199–208.
6. Korsvik C, Patil S, Seal S, Self S. Superoxide dismutase mimetic properties exhibited by vacancy engineered ceria nanoparticles. *Chem Commun (Camb)*. 2007;(10):1056–1058.
7. Chandar KN, Jayavel R. Synthesis and characterization of CTAB passivated cerium oxide nanoparticles prepared by co-precipitation route. *Physica E*. 2014;58:48–51.
8. Darroudi M, Hoseini SJ, Oskuee RK, Hosseini HA, Gholami L, Gerayli S. Food-directed synthesis of cerium oxide nanoparticles and their neurotoxicity effects. *Ceram Int*. 2013;40(5):7425–7430.
9. Renu G, Divya Rani VV, Nair SV, Subramanian KRV, Lakshmanan VK. Development of cerium oxide nanoparticles and its cytotoxicity in prostate cancer cells. *Adv Sci Lett*. 2012;6:17–25.
10. Arumugam A, Karthikeyan C, Hameed ASH, Gopinath K, Gowri S, Karthika V. Synthesis of cerium oxide nanoparticles using Gloriosa superba L. leaf extract and their structural, optical and antibacterial properties. *Mater Sci Eng C Biol Appl*. 2015;49:408–415.
11. Yu S-H, Cölfen H, Fischer A. High quality CeO nanocrystals stabilized by a double hydrophilic block copolymer. *Colloids Surf A Physicochem Eng Asp*. 2004;243(1–3):49–52.
12. Channei D, Inceesungvorn B, Wetchakun N, et al. Photocatalytic activity under visible light of Fe-doped CeO nanoparticles synthesized by flame spray pyrolysis. *Ceram Int*. 2012;39(3):3129–3134.
13. Lin HL, Wu CY, Chiang RK. Facile synthesis of CeO nanoplates and nanorods by [100] oriented growth. *J Colloid Interface Sci*. 2010; 341(1):12–17.
14. Sreeremya TS, Thulasi KM, Krishnan A, Ghosh S. A novel aqueous route to fabricate ltrasmall monodisperse Lipophilic Cerium oxide Nanoparticles. *Ind Eng Chem Res*. 2012;51(1):318–326.
15. Godinho MJ, Gonçalves RF, Santos LPS, Varela JA, Longo E, Leite ER. Room temperature co-precipitation of nanocrystalline CeO and CeGdO powder. *Mater Lett*. 2006;61(8–9):1904–1907.
16. George S, Pokhrel S, Xia T, et al. Use of a rapid cytotoxicity screening approach to engineer a safer zinc oxide Nanoparticle through iron Doping. *ACS Nano*. 2010;4(1):15–29.
17. Soni MG, Burdock GA, Christian MS, Bitler CM, Crea R. Safety assessment of aqueous olive pulp extract as an antioxidant or antimicrobial agent in foods. *Food Chem Toxicol*. 2006;44(7):903–915.
18. UN Food and Agriculture Organization. *Yearbook Production*. Rome: FAO; 1995;48:118–119.
19. Omar SH. Oleuropein in olive and its pharmacological effects. *Sci Pharm*. 2010;78(2):133–154.
20. Japón-Luján R, Luque-Rodríguez JM, Luque de Castro MD. Dynamic ultrasound-assisted extraction of oleuropein and related biophenols from olive leaves. *J Chromatogr A*. 2006;1108(1):76–82.
21. Benavente-García O, Castillo J, Lorente J, Ortuño A, Del Rio JA. Antioxidant activity of phenolics extracted from L. leaves. *Food Chem*. 2000; 68(4):457–462.
22. Maneerung T, Tokura S, Rujiravanit R. Impregnation of silver nanoparticles into bacterial cellulose for antimicrobial wound dressing. *Carbohydr polym*. 2008;72(1):43–51.
23. Ahmed S, Ahmad M, Swami BL, Ikram S. A review on plants extract mediated synthesis of silver nanoparticles for antimicrobial applications: a green expertise. *J Adv Res*. 2016;7(1):17–28.
24. Thakkar KN, Mhatre SS, Parikh RY. Biological synthesis of metallic nanoparticles. *Nanomedicine*. 2010;6(2):257–262.
25. Abbas F, Iqbal J, Jan T, et al. Differential cytotoxicity of ferromagnetic Co doped CeO nanoparticles against human neuroblastoma cancer cells. *J Alloys Compd*. 2015;648:1060–1066.
26. Khan SB, Faisal M, Rahman MM, Jamal A. Exploration of CeO nanoparticles as a chemi-sensor and photo-catalyst for environmental applications. *Sci Total Environ*. 2011;409(15):2987–2992.
27. Gao J, Zhao Y, Yang W, et al. Preparation of samarium oxide nanoparticles and its catalytic activity on the esterification. *Mater Chem Phys*. 2003;77(1):65–69.
28. Goharshadi EK, Samiee S, Nancarrow P. Fabrication of cerium oxide nanoparticles: Characterization and optical properties. *J Colloid Interface Sci*. 2011;356(2):473–480.
29. Maensiri S, Masingboon C, Laokul P, et al. Egg white synthesis and photoluminescence of platelike clusters of CeO_2 nanoparticles. *Cryst Growth Des*. 2007;7(5):950–955.
30. Suresh R, Ponnuswamy V, Mariappan R. Effect of annealing temperature on the microstructural, optical and electrical properties of CeO_2 nanoparticles by chemical precipitation method. *App Surf Sci*. 2013; 273:457–464.
31. Faik ON, Mehmet Y, Denisa F, Anton F, Florica D, Alexandra P. Molecular mechanism and targets of the Antimicrobial activity of metal Nanoparticles. *Cur Top Med Chem*. 2015;15(16):1583–1588.
32. Lima R, Seabra AB, Durán N. Silver nanoparticles: a brief review of cytotoxicity and genotoxicity of chemically and biogenically synthesized nanoparticles. *J App Toxicol*. 2012;32(11):867–879.
33. Aziz NH, Farag SE, Mousa LA, Abo-Zaid MA. Comparative antibacterial and antifungal effects of some phenolic compounds. *Microbios*. 1998;93(374):43–54.
34. Furneri PM, Marino A, Saija A, Uccella N, Bisignano G. In vitro antimycoplasmal activity of oleuropein. *Int J Antimicrob Agents*. 2002;20(4): 293–296.
35. Hameed ASH, Karthikeyan C, Sasikumar S, Kumar S, kumaresan S, Ravi G. Impact of alkaline metal ions mg2+, ca2+, Sr2+ and Ba2+ on the structural, optical, thermal and antibacterial properties of ZnO nanoparticles prepared by the co-precipitation method. *J Mater Chem B*. 2013;1(43):5950–5962.
36. Xia T, Kovochich M, Liong M, et al. Comparison of the mechanism of toxicity of zinc oxide and cerium oxide nanoparticles based on dissolution and oxidative stress properties. *ACS Nano*. 2008;2(10): 2121–2134.
37. Burello E, Worth AP. A theoretical framework for predicting the oxidative stress potential of oxide nanoparticles. *Nanotoxicology*. 2011; 5(2):228–235.
38. Li Y, Zhang W, Niu J, Chen Y. Mechanism of photogenerated reactive oxygen species and correlation with the antibacterial properties of engineered metal-oxide Nanoparticles. *ACS Nano*. 2012;6(6):5164–5173.
39. Tong G-X, Du F-F, Liang Y, et al. Polymorphous ZnO complex architectures: Selective synthesis, mechanism, surface area and Zn-polar plane-codetermining antibacterial activity. *J Mater ChemB*. 2012;1(4):454–463.
40. Wang X, Yang F, Yang W, Yang X. A study on the antibacterial activity of one-dimensional ZnO nanowire arrays: effects of the orientation and plane surface. *Chem Commun (Camb)*. 2007;(42):4419–4421.
41. Stylianou M, Kulesskiy E, Lopes JP, Granlund M, Wennerberg K. Antifungal application of Nonantifungal drugs. *Antimicrob Agents Chemother*. 2014;58(2):1055–1062.
42. Howlett NG, Avery SV. Induction of lipid peroxidation during heavy metal stress in Saccharomyces cerevisiae and influence of plasma membrane fatty acid unsaturation. *Appl Environ Microbiol*. 1997;63(8):2971–2976.